Biochimica et Biophysica Acta 1840 (2014) 3264–3276

Contents lists available at ScienceDirect

Biochimica et Biophysica Acta

journal homepage: www.elsevier.com/locate/bbagen

Synthesis and characterization of Cu/Ag nanoparticle loaded mullite nanocomposite system: A potential candidate for antimicrobial and therapeutic applications

S. Kar [a], B. Bagchi [b], B. Kundu [c], S. Bhandary [d], R. Basu [e], P. Nandy [f], S. Das [a,*]

[a] Physics Department, Jadavpur University, Kolkata 700 032, India
[b] Fuel Cell and Battery Division, Central Glass and Ceramic Research Institute, Kolkata 700 032, India
[c] Biotechnology Department, IIT Kharagpur, Kharagpur 721302, India
[d] Bose Institute, Department of Molecular Medicine, Kolkata 700 054, India
[e] Physics Department, Jogamaya Devi College, Kolkata 700 026, India
[f] Centre for Interdisciplinary Research and Education, Kolkata 700 068, India

ARTICLE INFO

Article history:
Received 21 December 2013
Received in revised form 6 May 2014
Accepted 15 May 2014
Available online 1 August 2014

Keywords:
Mullite
Metal nanoparticle
Antibacterial activity
Cyto-compatibility

ABSTRACT

Background: Microbial resistance to antibiotics has triggered the development of nanoscale materials as an alternative strategy. To stabilize these particles an inert support is needed.
Method: Porous nanomullite developed by sol–gel route is loaded with copper and silver nanoparticle by simple adsorption method. These nanocomposites are characterized using XRD, FTIR, TEM, SEM, EDAX and UV–visible spectrophotometer. Antibacterial activity of these nanocomposites against Gram positive and Gram negative bacteria are performed by bactericidal kinetics, flow cytometry and MTT assay. The underlying mechanisms behind the antimicrobial property and cell death are also investigated by EPR spectroscopy, intracellular ROS measurement and β-galactosidase assay. The cytocompatibility of the nanocomposites is investigated by cell viability (MTT), proliferation (Alamar blue) and wound healing assay of mammalian fibroblast cell line.
Results: Nanocomposites show a fairly uniform distribution of metal nanoparticle within mullite matrix. They show excellent antibacterial activity. Metal ions/nanoparticle is found to be released from the materials (CM and SM). Treated cells manifested high intracellular oxidative stress and β-galactosidase activity in the growth medium. The effect of nanocomposites on mammalian cell line depends on exposure time and concentration. The scratch assay shows normal cell migration with respect to control.
Conclusion: The fabricated nanoparticles possess diverse antimicrobial mechanism and exhibit good cytocompatibility along with wound healing characteristics in mouse fibroblast cell line (L929).
General significance: The newly synthesized materials are promising candidates for the development of antimicrobial ceramic coatings for biomedical devices and therapeutic applications.

1. Introduction

Excessive use of antibacterial agents like chemically modified natural compounds (penicillins, cephalosporins or carbapenems), pure natural products (aminoglycosides) and purely synthetic antibiotics lead to the development of drug resistant microbes. These resistant pathogens cause the emergence of diseases, which are difficult to diagnose and control. This has prompted the development of alternative antimicrobial agents such as nanoscale materials. Because of their extremely small size and high surface to volume ratio, nanoparticles have increased activity and interaction with microbial components. Additionally, the antimicrobial mechanism of metal nanoparticles is diverse, restricting the easy development of microbial resistance [1].

Silver and its compounds are popular antimicrobial agents. Silver nanoparticles are now used in a wide spectrum of consumer products right from clothing, respirators, antibacterial sprays, detergent, socks, shoes, etc. Silver based nanoparticles are being used in various forms such as metallic silver nanoparticles, silver chloride particles, silver impregnated zeolite, powders or polymer silver nanoparticle composites [2]. Copper nanoparticles enjoy much attention because of their catalytic, optical, electrical and antifungal/antibacterial applications [3]. However, optimal use of metal nanoparticles as antibacterial agents is limited due to their low stability like, light induced deactivation of silver nanoparticles and aerial oxidation of copper nanoparticles. In addition, nanoparticles tend to aggregate to larger particles reducing their performance. Therefore, to increase the stability of these particles and reduce

* Corresponding author. Tel.: +91 9433091337.
E-mail address: sukhendasju@gmail.com (S. Das).

http://dx.doi.org/10.1016/j.bbagen.2014.05.012
0304-4165/

their toxic effect on human, a solid porous inert support is ideal, which inhibits the aggregation, resulting in a slow and prolonged release for long term and recurrent use. Moreover, these nanoparticle loaded supports provide the attachment sites for microbes, which then comes in intimate contact with the surface adsorbed nanoparticles.

Mullite ceramic based antimicrobial agents are a new breed of materials, which have tremendous potential in the biomedical field due to their non toxic nature, biocompatibility and high mechanical strength [4]. Antibacterial biofilm activity of doped (zinc and silver) or adsorbed (copper) mullite aggregates against *Pseudomonas aeruginosa* has already been established [5,6]. Therefore, we hypothesize that porous mullite substrates are ideal for entrapping metal nanoparticles for antimicrobial applications. In the present work, a porous nanocrystalline mullite composite is synthesized by sol–gel process and is loaded with copper and silver nanoparticles by simple adsorption. Antimicrobial activity of these composites is then evaluated. Finally the biocompatibility and wound healing assays are performed in mammalian fibroblast cell line for establishing its potentiality as antimicrobial ceramic coating and for therapeutic applications.

2. Experimental

2.1. Materials

Aluminium isopropoxide (Loba Chemie), TEOS (Merck Germany), Ethanol, Copper chloride dihydrate pure ($CuCl_2.2H_2O$) (>98% pure, Merck, India), Silver Nitrate, Hydrazine hydrate ($NH_2NH_2.H_2O$) (99% pure, Merck, India), Cetyl Trimethyl Ammonium Bromide (CTAB), Beef extract, Peptone, Yeast extract, Agar (Himedia Pvt. Ltd., India), 3(4,5-dimethylthiazol-2-yl)—2,5-diphenyl tetrazolium bromide (MTT), ONPG (SRL), SYBR® Green, Propidium iodide, 2′,7′-Dichlorofluorescin diacetate (sigma-aldrich), Dulbecco's Modified Eagle's Medium (DMEM), trypsin–EDTA, penicillin/streptomycin and fetal bovine serum (Gibco, Invitrogen, USA), Alamar blue dye (AbD Serotec, UK), Tissue culture grade polystyrene flasks and cell culture plates (Tarsons, India). Bacterial cultures (*Staphylococcus aureus* MTCC-96 and *Escherichia coli*, MTCC-1652) were procured from Microbial type cell culture (MTCC) Chandigarh, India.

Mouse fibroblast cell line-L929 was obtained from the National Centre for Cell Science, Pune, India.

2.2. Methods

2.2.1. Synthesis of nanoporous mullite

Mullite was synthesized by sol–gel process using aluminium isopropoxide and tetra ethyl ortho silicate (TEOS) as starting material [7]. Briefly 15.32 g of aluminium isopropoxide was dispersed in ethanol (99.99% pure) and mixed by stirring in a magnetic stirrer. This was followed by addition of 5.21 g of TEOS with a micropipette and the stirring is continued for 24 h at 35 °C. The solution was then stirred for 2 h at 60 °C and thereafter hydrolyzed by adding 20 ml of distilled water. The gel thus obtained was dried at 70 °C in the oven. The mullite precursor thus formed was powdered by crushing and was sintered at 1300 °C in the furnace for 4 h.

2.2.2. Synthesis of copper and silver nanoparticle

Copper and silver nanoparticles were synthesized by reduction of copper chloride and silver nitrate respectively with hydrazine hydrate using 0.1 M CTAB as coating agent. Ammoniacal copper chloride $[Cu(NH_3)_4(H_2O)_2]^{2+}$ was prepared by dropwise addition of ammonia solution to 0.1 M copper chloride solution (in deionized water) until a transparent blue solution was formed (pH ~ 10). 0.1 M silver nitrate was used for the preparation of silver nanoparticles. In a test tube 600 μl of the CTAB stock was mixed with 20 μl of hydrazine. To the reaction mixture 150 μl of copper complex solution and silver nitrate solution was added in stirring condition. The volume was adjusted to 6 ml with deionized water. The reaction was carried out in inert nitrogen atmosphere to minimize aerial oxidation. The mixture was then allowed to stand for 30 min. The appearance of wine red color solution indicated the formation of copper nanoparticles. For silver nanoparticles the reaction was much faster. Transparent yellow colored solution appeared immediately after the components were added, indicating the formation of silver nanoparticles.

2.2.3. Synthesis of porous mullite–nanoparticle composite

Porous mullite with copper and silver nanoparticle composite was synthesized by mixing the nanoparticles with mullite nanoparticles dispersed in water. Initially 400 mg of mullite was dispersed in 20 ml of distilled water by stirring for 30 min at room temperature. To the dispersion, 12 ml of the synthesized copper and silver nanoparticles was separately added and was then further stirred for 1 h. The suspension was then centrifuged at 15,000 *g* for 10 min and washed three times with distilled water to remove the free CTAB. The pellet obtained was dried in vacuum and copper nanoparticle–mullite (CM) and silver nanoparticle–mullite (SM) were obtained. The nanocomposites were stored in normal laboratory conditions for 3 months after which the following experiments were performed.

2.2.4. X-ray diffraction (XRD)

Powder X-ray diffraction (XRD) patterns were recorded using a Bruker AXS (Model D8, WI, USA) setup with CuKα radiation (1.5409 Å) and scan speed of 5 min^{-1} and scanning range from 10^0 to 70^0 (2θ).

2.2.5. Fourier transform infrared spectroscopy (FTIR)

Fourier transform infrared spectroscopy was performed by FTIR-8400S model Shimadzu, Tokyo. Samples were prepared by KBr disk method [8], in which 0.2 g of KBr (spectroscopy grade) was thoroughly mixed with sintered sample powder (1% by weight of KBr) and then made into disks by uniaxial pressing. Scanning range was set from 400 to 2000 cm^{-1} under Happ–Genzel configuration.

2.2.6. UV–visible spectrophotometer

UV-visible spectrophotometer (Lambda 25, Perkin Elmer, USA) was used to study the absorption spectra of the composite CM and SM.

2.2.7. Scanning electron microscopy, energy dispersive X-ray analysis (EDAX) and BET

Morphological characteristics of the mullite were observed by scanning electron microscope (SEM) model FEI Quanta 250 (USA) and E-DAX analysis. A minute quantity of the sample was directly placed on carbon coated grid, sputter coated with gold and then observed by SEM. Surface area of CM and SM were determined by N_2 adsorption using BET method (Beckman Coulter SA-3100 surface area analyzer, USA).

2.2.8. Transmisson electron microscopy

The particle size of synthesized nanomullite was observed by JEM-2100 HRTEM model. A minute quantity of the sample was dispersed in water by sonication and observed under the microscope.

2.2.9. Antibacterial activity

2.2.9.1. Determination of MBC and MIC. The minimum inhibitory concentration (MIC) was determined by treating approximately 10^7 CFU/ml cells from overnight grown culture in log phase. *E. coli* (MTCC-1652) and *S. aureus* (MTCC-96) were treated with 1–10 mg/ml of mullite (M), CM and SM. The same process was also followed by treating bacteria with 2 μl–300 μl/ml of synthesized copper and silver nanoparticles to compare their effect with respect to the mullite as well as the nanocomposites. All the culture broths were incubated overnight at 37 °C. MIC is defined by the concentration of the material that exhibits no visible growth.

Minimum bactericidal concentration (MBC) was determined by plating all the higher doses of the material showing no visible growth above MIC. MBC is that concentration of the material which kills almost 99% of the bacteria in nutrient agar plate after 24 h incubation while the untreated control was considered as 100%.

2.2.9.2. Bactericidal kinetics. Bactericidal kinetics of the two synthesized composites CM and SM were determined using *S. aureus* and *E. coli*. From an overnight growing fresh culture of bacteria, a volume of culture approximately representing ~10^7 CFU/ml was washed and suspended in PBS buffer. The fresh culture was then diluted and inoculated in 5 ml nutrient broth (0.5% peptone, 0.1% beef extract, 0.2% yeast extract, 0.5% NaCl, pH 7) at a final cell concentration of 10^4 CFU/ml. For antibacterial assay 3 mg/ml (~2 × MIC) of CM and SM are used to treat the inoculated broth. For comparison *E. coli* and *S. aureus* were also treated with CuNps and AgNps at their respective MIC values using same cell concentration. Mullite was not used in subsequent antibacterial studies due to its poor antibacterial effect as observed in earlier experiments. An untreated but inoculated broth was used as positive control. Time dependent killing was determined by plating the culture from the treated sample and control in agar plate (1.8%) at 0, 0.5, 1.5, 3 and 4 h. Plates were incubated at 37 °C and number of colonies was counted after 24 h. The whole experiment was repeated thrice to reproduce the data. The antibacterial effect was calculated using the equation:

$$M(\%) = [(B\text{-}C/B)] \times 100,$$

Where, M is the mortality rate (%), B is the mean number of bacteria in the control samples (CFU/sample) and C is the mean number of bacteria on the treated samples (CFU/sample).

2.2.10. Flow cytometry

Flow cytometry analysis was done according to the method followed by Joshi et al. 2010 [9]. Briefly *E. coli* and *S. aureus* were grown to mid log phase in nutrient broth. The overnight culture was centrifuged at 6000 *g* for 10 min and followed by washing it three times with buffer (10 mM Tris, pH 7.4). The bacterial suspension was then inoculated in 5 ml of fresh broth with approximately 10^4 CFU/ml and treated with 15 mg of CM and SM for 4 h. Untreated culture was set as control. After 4 h the bacterial suspension was centrifuged and washed in tris buffer. Propidium iodide (PI) at concentration of 10 μg/ml was used to fix the suspension for 15 min. A Becton-Dickinson FACS Verse double laser cytometer was used to obtain flow cytometric reading using 488 nm excitation and bandpass filters.

2.2.11. MTT assay

Bacterial viability assay was performed by using MTT [3(4,5-dimethylthiazol-2-yl)-2,5-diphenyl tetrazolium bromide] [10]. Overnight grown bacterial culture was harvested after centrifugation and washing in PBS (pH 7.4). Bacterial cells were then treated with 15 mg of the antimicrobial material (CM and SM) at 10^4 CFU/ml cell concentration. For comparison bacteria at the same concentration were treated with CuNp and AgNp at their MIC concentration. After 4 h of incubation cells were washed and suspended in PBS. MTT stock (5 g/L) at 1:10 dilution was

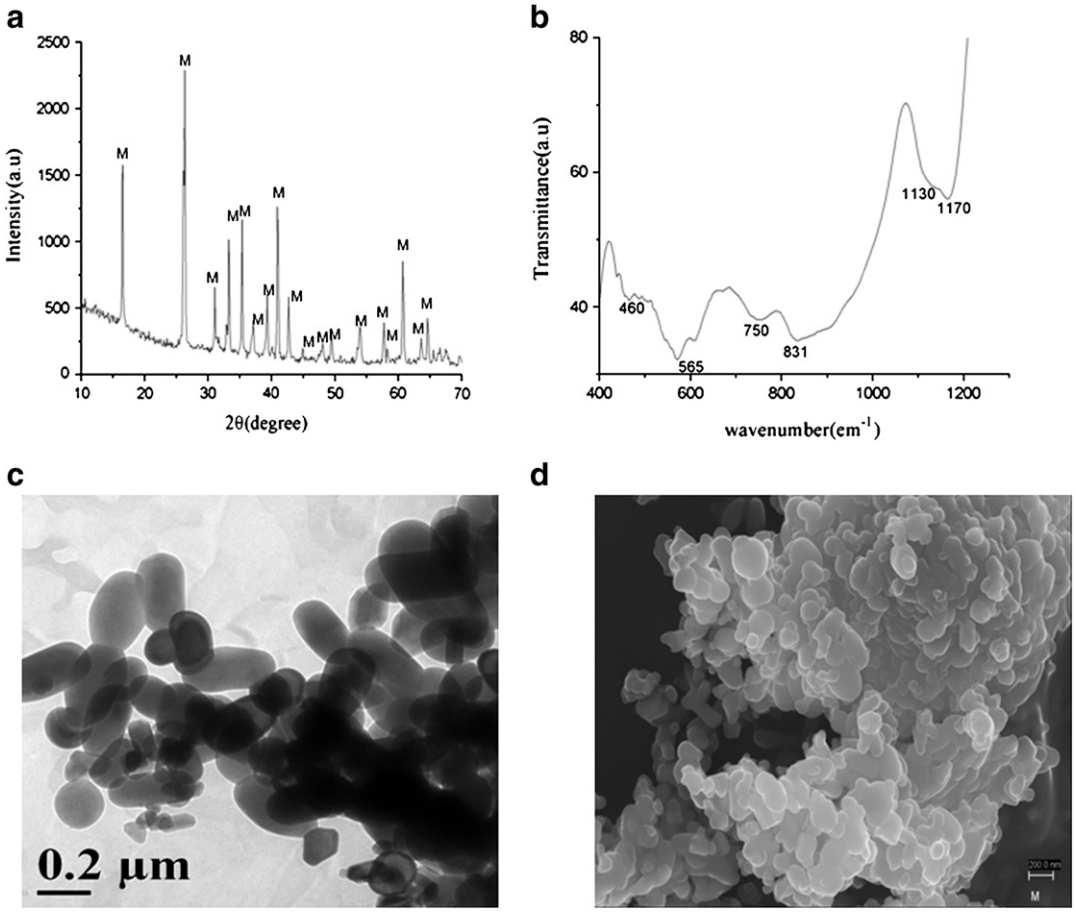

Fig. 1. Characterization of nanomullite by (a) XRD, (b) FTIR, (c) TEM, (d) FESEM.

added and the cells were incubated for 1 h. After this the suspension was centrifuged (10,000 *g*, 1 min) and formazan formed was dissolved in 500 μl DMSO. The intensity of the formazan formed was measured spectrophometrically at 540 nm.

2.2.12. Inner membrane permeabilization assay

Membrane integrity and permeation of inner membrane were studied by the treatment of bacteria with CM and SM. The assay is based on the fact that chromogenic dye ONPG (o-nitrophenyl-ß-D-galactoside) is a substrate for β-galactoside and produces galactose and yellow O-nitrophenol, the intensity of the latter is measured at 420 nm [11]. Therefore the disruption of the bacterial inner membrane was understood with a significant increase in absorbance of the supernatant of the treated sample compared to the control.

E. coli DH5α strain with PUC was chosen for the study. Bacteria was grown overnight in ampicillin nutrient agar plate. A single colony was inoculated in fresh nutrient broth containing IPTG, which acts as an inducer for the expression for β-galactosidase enzyme. The overnight grown culture was washed with distilled water. Equal amounts of the cells were treated with nanocomposites and incubated at 37 °C for 4 h. Thereafter the bacterial culture was reacted with ONPG for 15 min and absorbance was recorded at 420 nm.

2.2.13. Bacterial sample preparation for FESEM

Overnight grown bacterial culture was harvested and inoculated with approximately 10^4 cells. 15 mg of the nanocomposites was used to treat the bacterial culture and incubated for 4 h. Untreated but inoculated culture was set as control. A very minute amount of the sample was placed on the cover slip and dried in air and placed on a carbon tape.

2.2.14. Reactive oxygen generation (ROS) detection and fluorescence microscopy

The burst of superoxide radical was measured according to Su et al. 2009 [12]. In brief, overnight grown bacteria (*E. coli* and *S. aureus*) at log phase were washed with PBS buffer (pH: 7.4). Fresh broth was inoculated with approximately 10^4 CFU/ml and treated with 3 mg/ml of CM and SM. For comparison an equal number of cells was also treated with CuNps and AgNps at their MIC values. The cultures were allowed to grow in 37 °C for 1 h. Untreated sample was taken as control. Bacteria were then treated with 10 μM DCFHDA for 30 min followed by washing

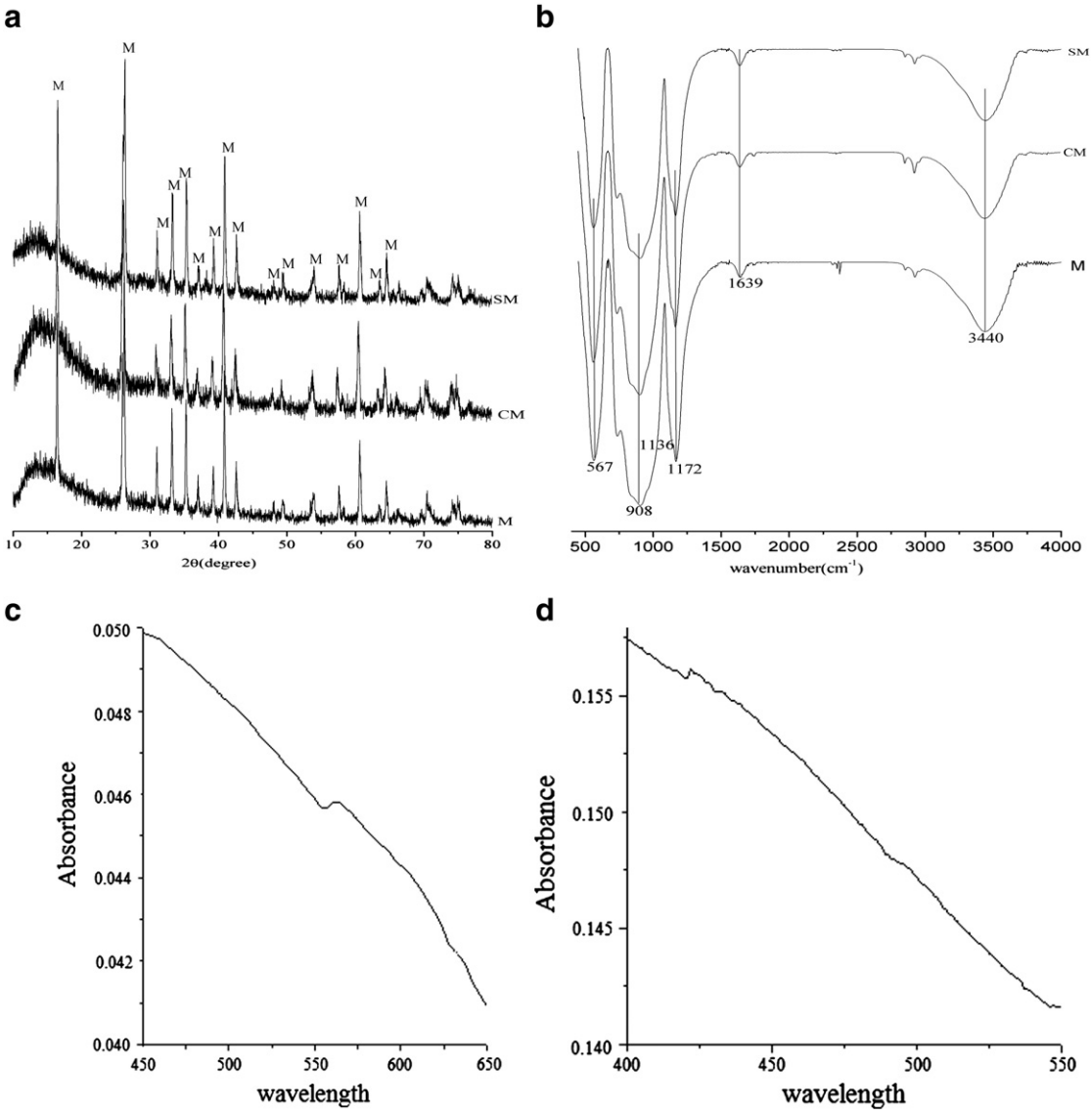

Fig. 2. Characterization of copper mullite and silver mullite respectively by XRD and FTIR (a, b), absorbance spectrophotometer (c, d) respectively.

Table 1
FTIR frequency assignments of mullite.

Wavenumber (cm^{-1})	Band assignments
1170 (strong)	$_{as}$Si – O – Si of SiO_4
1130 (shoulder)	$_{as}$ Si – O – Al
750 (shoulder)	(AlO_4)
831 (strong)	(AlO_4)
565 (strong)	(AlO_6)
460 (weak)	δSiO_4

in PBS buffer. The ROS level was measured by fluorescence spectrophotometer with excitation at 490 nm and emission at 520 nm.

SYBR Green and PI were used for fluorescence microscopic analysis of live and dead cells. The principle of staining is based on the fact that SYBR Green is a cell membrane permeant dye that stains both live and dead cells whereas PI is an impermeant dye that stains only dead and membrane compromised cells. An interesting phenomenon that takes place in this dye system, is fluorescence quenching of cell permeant dye SYBR Green by PI when both of them are staining nucleic acid. Intact live cells will appear green whereas dead cells will appear red when observed under fluorescence microscope. The staining process followed is according to the method reported by Berbesti et al. [13].

SYBR Green was diluted to 1:100 v/v in DMSO from the stock and used as working solution. PI was diluted to 1 mg/ml in deionized water and used as stock solution. Bacterial samples were prepared as stated above. To 1 ml of each treated and untreated sample 10 μl each of SYBR Green (final concentration 1:10000) and PI (10 μg/ml final concentration) were added. Samples were incubated at 37 °C for 15 min The cells were then immediately mounted on slides and observed under fluorescence microscope (Motic Image plus 2.0 software) for analysis.

2.2.14.1. Electron spin resonance spectroscopy. EPR spectra were obtained by a JEOL spectrophotometer (JES FA200). Small amounts of CM and SM were dispersed in deionized water and allowed to settle. The supernatant was run at 77 K in a liquid nitrogen finger dewar keeping power 1 mW, microwave frequency 9.2 GHz and center field 315 mT.

2.2.15. Cytocompatibility study

2.2.15.1. Maintenance of cell line. The mouse fibroblast cell line (L929) was cultured in DMEM medium supplemented with 10% FBS and 100 U/mL penicillin–streptomycin at 37 °C and 5% CO_2 humidified atmosphere. At confluence, cells were washed with sterile phosphate buffered saline (PBS pH 7.4), trypsinized and released into suspension to suitable cell density for further studies. Cells without any treatment/exposure to test compounds served as control.

2.2.15.2. Preparation of nanocomposites for cell culture. Higher stock solutions of nanocomposites (5 mg/ml) were prepared by dispersing CM and SM particles in sterile phosphate buffer (pH 7.4) and sonicating

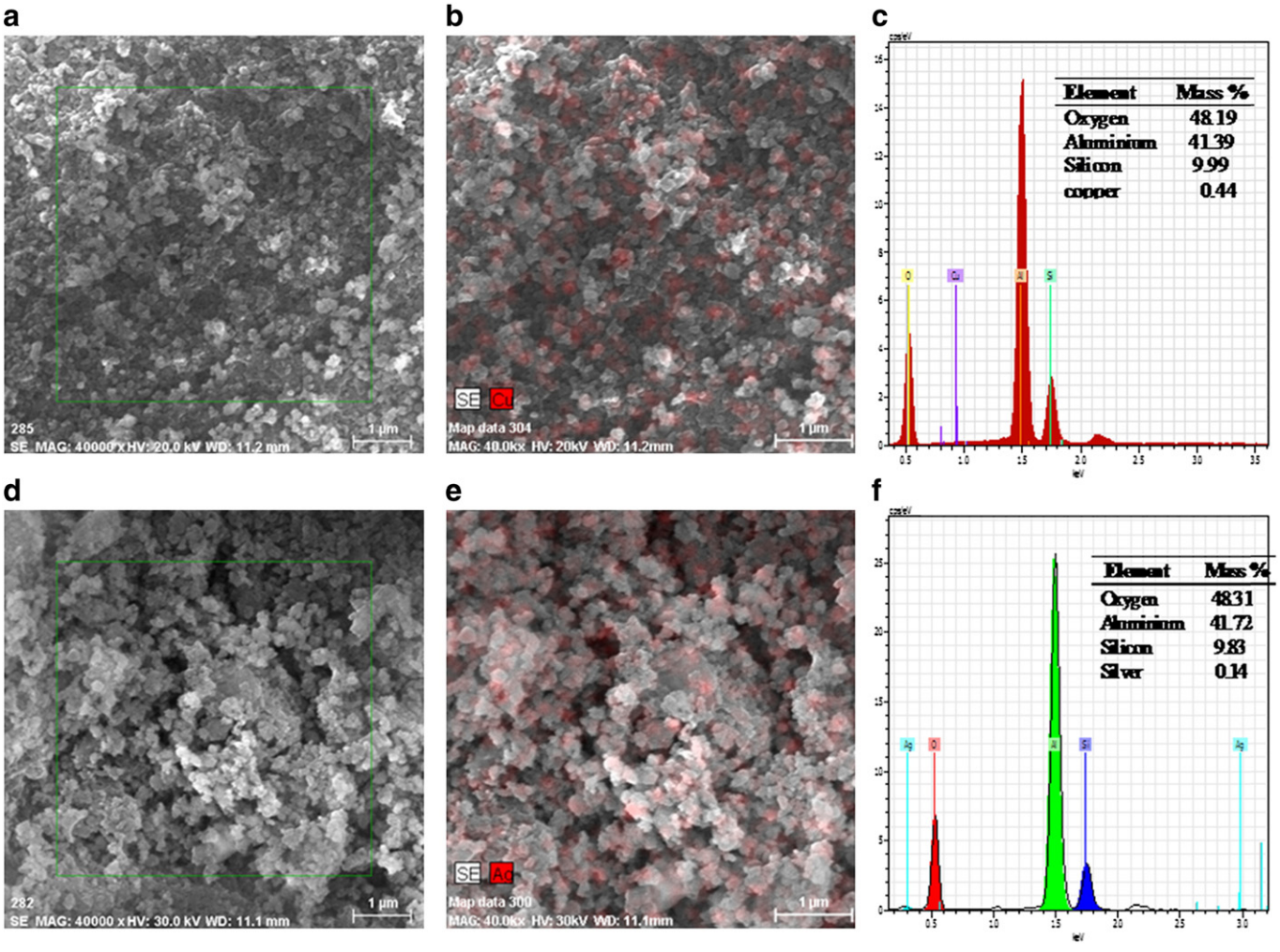

Fig. 3. SEM micrographs, atom mapping and EDAX analysis of CM (a, b, c) and SM (d, e, f) respectively. Mass percent as determined from EDAX analysis is shown in inset.

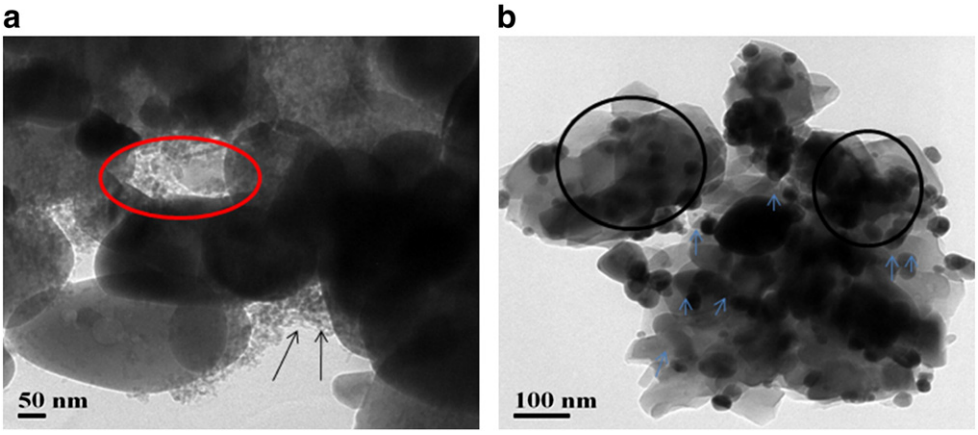

Fig. 4. TEM micrographs (a, b) for CM and SM respectively.

Table 2
MIC values of CM and SM with their corresponding copper and silver content against *E. coli* and *S. aureus*.

Bacteria	Mullite (mg/ml)	CuNp (μl/ml)	AgNp (μl/ml)	CM (mg/ml)	Cu content (μg/ml)	SM (mg/ml)	Ag content (μg/ml)
E. coli	8	8	12	1.4	6.6	1.6	13
S. aureus	8	10	10	1.2	5.65	1.5	12

for 30 min using a sonication bath at 37 °C. The solutions were then kept at 37 °C under sterile condition for 24 h for the release of the nanoparticles. Thereafter, the solutions were subjected to brief centrifugation (2000 *g* for 5 min) and the supernatant was diluted to desired concentrations (0.5–3 mg/ml) with complete DMEM for further cell culture studies.

2.2.15.3. MTT assay. To investigate any toxicity associated with the nano-composites under investigation (CM and M), cyto-toxicity assay (MTT) was performed using mouse fibroblast cell line-L929. Briefly, 10^5 cells/well of 96-well plate were seeded and allowed to adhere. The cell mono-layers were then treated with several dilutions (0.5–3 mg/ml) of CM and SM up to 24 h. At the end of each time point (12 and 24 h), 100 μL of freshly prepared MTT [5 mg/mL; 3-(4, 5-dimethylthiazol-2-yl)-2, 5-diphenyltetrazolium bromide; 5 mg/ml stock solution diluted into 1:10 in sterile phosphate buffer solution] was added into each well and incubated for 4 h at 37 °C and 5% CO_2 humidified atmosphere. The intracellular formazan crystals thus formed were solubilized in DMSO and the absorbance of the solution was measured at 595 nm using a micro-plate reader (Bio-Rad, USA).

2.2.15.4. Alamar blue assay. The effect of test nanocomposites on cellular proliferation was also evaluated by Alamar blue assay [14]. Briefly, cells after required treatment with test compounds (0.5–3 mg/ml as described above) were subjected to Alamar blue solution (stock diluted to 1:10 in complete cell culture media) and incubated for 4 h at 37 °C and 5% CO_2 humidified atmosphere. After incubation, the plates were read at 570/600 nm in a Multiskan spectrum (Thermo Scientific Multiskan Spectrum, Japan). The percentage of reduction in Alamar blue dye was calculated as per manufacture's protocol (AbD Serotec, UK).

2.2.15.5. Scanning electron microscopy (SEM). For SEM analysis, L929 cells seeded on coverslips were treated with the test samples (1 mg/ml) for 12 h. The cells, after treatment were washed once with sterile phosphate buffer saline and fixed in paraformaldehyde (4 v/v%) for one hour. The cells on coverslips were then dehydrated completely using series of alcohols (50–100%, each 20 min) and sputter coated with gold for SEM analysis (ZEISS EVO 60 scanning electron microscope, Germany).

2.2.15.6. Wound healing assay. The wound healing effect of the nanocomposites was assayed using L929 cells seeded in six-well plates (Nunc, Wiesbaden, Germany) in a density of 1×10^5 cells/well in growth medium and allowed to attain the confluence of about 90%. A scratch was then created in each well using sterile 200 μl pipet tips. The cells were washed thrice with PBS (pH 7.4) and then incubated with test materials (2.5 mg/ml for CM and 3 mg/ml for SM prepared in complete media) for 24 h at 37 °C and 5% CO_2. Cells incubated with complete media served as control. The scratches were documented under the phase-contrast microscope immediately after the creation of wound and after subsequent pre-determined time intervals (6, 18 and 24 h). The images taken at the same position were noted each time to monitor the repair process. The experiments were performed in duplicate and representative images are reported.

2.2.16. Statistical analysis

Data were presented as mean ± standard deviation (SD); n = 3, or otherwise mentioned. Single factor one-way statistical analysis was performed using ANOVA to determine statistical significance ($^*p < 0.05$).

Table 3
MBC values of CM and SM against *E. coli* and *S. aureus*.

Bacteria	Mullite	CuNp (μl/ml)	AgNp (μl/ml)	CM (mg/ml)	SM (mg/ml)
E. coli	–	8	12	4	5.6
S. aureus	–	10	10	3.6	5

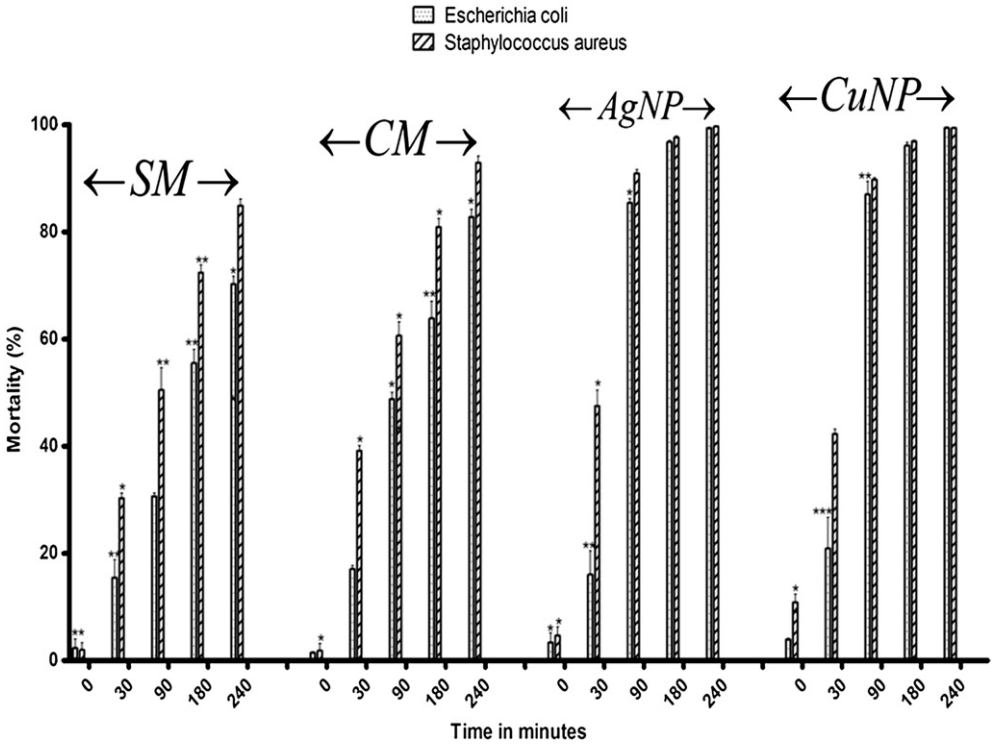

Fig. 5. Bactericidal kinetics representing time dependent mortality rate. Values are means ± SEM of 5 separate experiments done in triplicate. *p < 0.05, **p < 0.005, ***p < 0.0005. All p values denoted with * are significant at the 1% level compared to controls and error bars are standard error of the mean (N = 3).

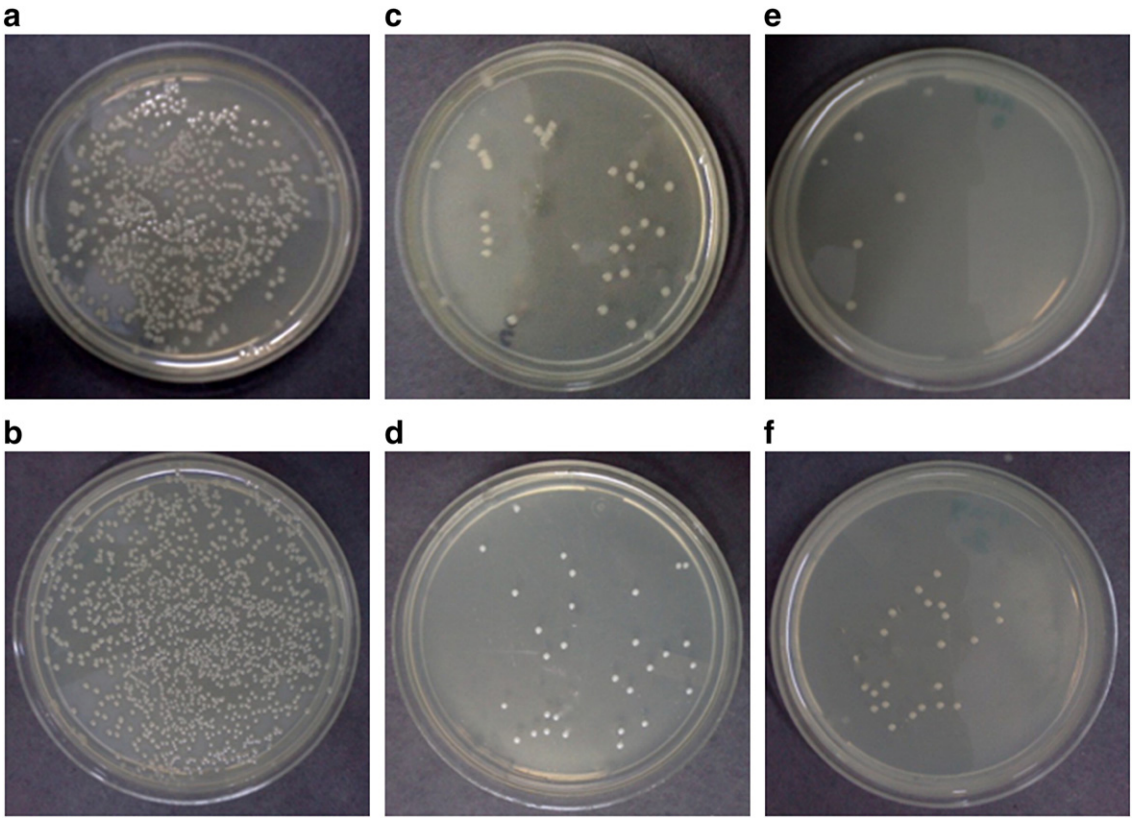

Fig. 6. Agar plate pictures of *E. coli* and *S. aureus* showing control, CM and SM treated for 4 h after overnight incubation at 37 °C.

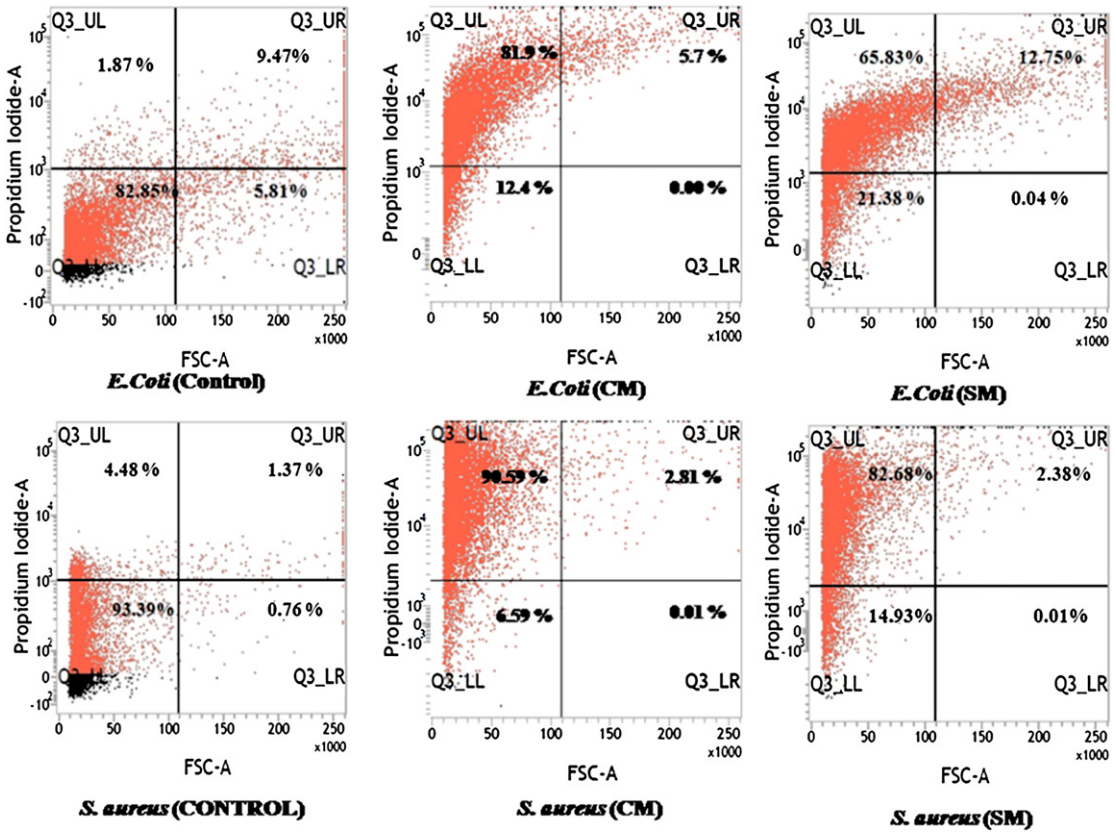

Fig. 7. Flow cytometry analysis of *E. coli and S. aureus* by propidium iodide (10 μg/ml) after 4 h of treatment with CM and SM with 10^4 CFU/ml cell concentration using 488 nm excitation and bandpass filters.

3. Results and discussion

3.1. XRD analysis

The X-ray diffraction pattern of the nanomullite shows prominent reflections indicating formation of well crystallized mullite phase. All the peaks correspond to mullite phase without any unreacted alumina or silica (Fig. 1a) [15]. The X-ray pattern of CM and SM exhibit no peak of copper and silver nanoparticles even at low scan speed, which is due to the fact that the amount of nanoparticles in the composite is very low, below the detection limit (Fig. 2a).

3.2. FTIR

The FTIR spectrum of the mullite powder represents the vibrations of the chemical bonds at different wavenumbers (Fig. 1b). The strong peak near 1170 and the shoulder at 1130 cm^{-1} is assigned to asymmetric stretching vibration of the Si – O – Si of SiO_4 tetrahedra of mullite and Si – O – Al respectively. The band at 831 cm^{-1} represents stretching vibration of tetrahedrally coordinated of Al – O bond (AlO_4). The peaks at around 565 cm^{-1} and 750 cm^{-1} are due to the octahedrally coordinated aluminium atom. The peak at around 460 cm^{-1} is assigned to the bending of SiO_4 bonds [16]. The band assignments are listed in Table 1. FTIR spectra show no shifting of bands in CM and SM with respect to the mullite. However all the bands of mullite were present in the composite which is due to the low amount of particle within the composite (Fig. 2b).

3.3. UV–visible spectroscopy

Absorption spectra of CM and SM show characteristic bands at 560 nm and 430 nm (Fig. 2 c, d) due to the surface plasmon of copper nanoparticle and silver nanoparticle respectively, present in the mullite based composite. Since the metal nanoparticles are attached to the surface, plasmon bands are very difficult to observe in CM and SM due to scattering effect from the mullite aggregates [6].

3.4. Electron micrographs, EDAX and surface area (BET)

TEM micrographs of the dispersed mullite show particle size of varying range, about 100–300 nm, with very few particles of larger dimension of about 400 nm, probably formed by agglomeration of smaller particles (Fig. 1c). This is also supported by the SEM micrograph (Fig. 1d). As observed in the SEM and TEM images, the shapes of the particles are mostly oval with a few elongated grains.

TEM micrographs of the CM and SM also reveal uniform distribution of the copper and silver nanoparticles on the nanomullite grains. Copper nanoparticles show ultrafine dimension of around 5–10 nm (shown by red circle and black arrow) while silver nanoparticles are relatively larger (blue arrow) (40–50 nm) (Fig. 4a,b). However in the case of the TEM micrograph of CM a few copper nanoparticles are not seen to be interspersed within the matrix and look like individual particles. These were probably dislodged from the mullite matrix as a result of ultrasonication process during the sample preparation.

The EDAX spectra show the relative composition of the CM and SM (Fig. 3c,3f) and is presented in the table as an inset within the figure. Atom mapping of CM and SM for copper and silver atoms respectively, shows a fairly good distribution within the mullite matrix (3b,3e).

The surface area as measured by BET technique also indicates nano sized dimension of mullite with a value of 17.352 m^2/g. However, CM (17.652 m^2/g) and SM (17.231 m^2/g) show nominal difference in surface area. Thus adsorption of the nanoparticles does not adversely affect the surface properties of the mullite nanocomposite.

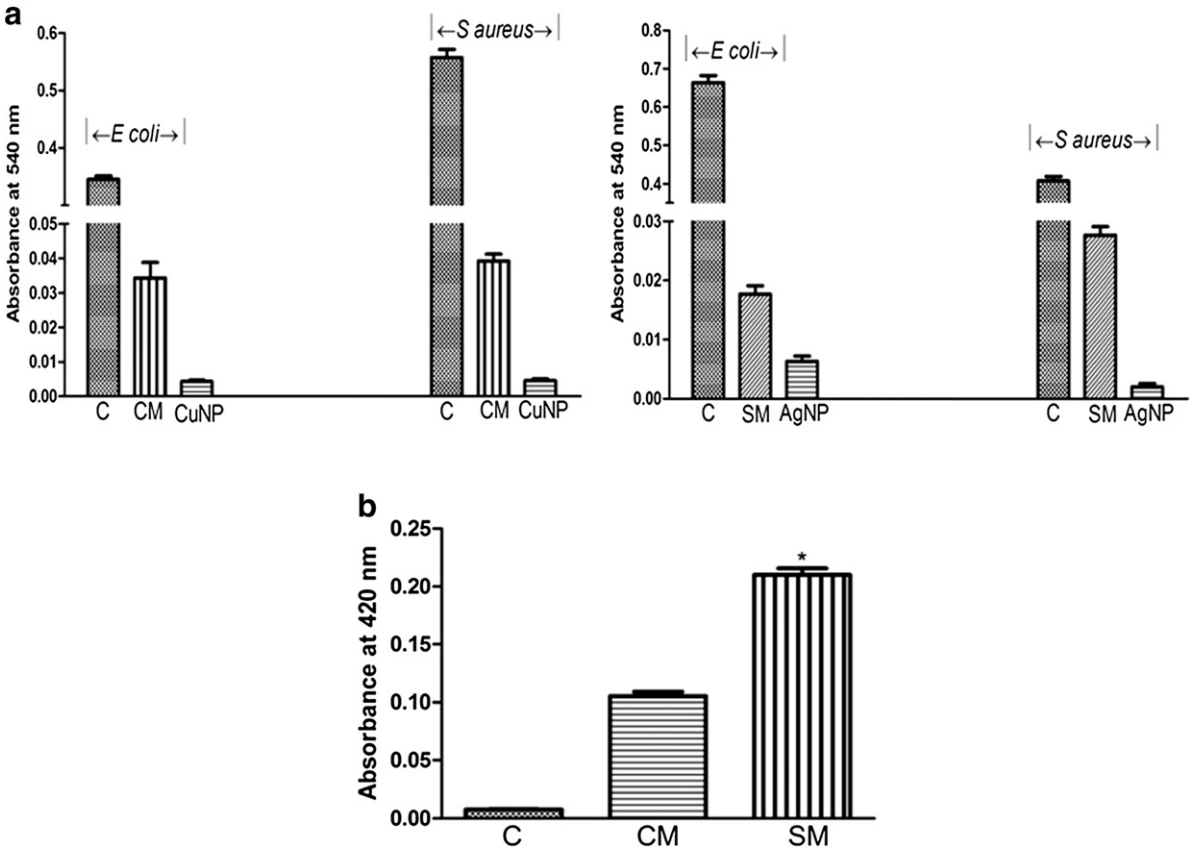

Fig. 8. (a) MTT bacterial cell viability assay. Statistical analysis of relative absorbance of microbial cells viability on treated CM, SM, AgNp and CuNp with respect to control. Error bar shows the standard error of mean (N = 3). (b) Inner membrane permeabilization assay.

3.5. Antibacterial activity

3.5.1. MIC & MBC

The antibacterial property of the two synthesized nanocomposites (CM and SM) is tested to determine the MBC and MIC. The MIC and MBC values are presented in form of Tables 2 and 3. The MIC values of the Gram negative bacteria *E. coli* are more than those of the Gram positive *S. aureus*.

The MBC for CM, SM and Cu/Ag nanoparticle treated cells are not more than 4 times their respective MIC values indicating that the nanocomposites are bactericidal rather than bacteriostatic.

3.5.2. Bactericidal kinetics

The bactericidal kinetics of exponentially growing *E. coli* and *S. aureus* are checked against CM and SM by time kill assay. The result conveys that within 4 h of incubation period the population of *S. aureus* for CM and SM is reduced by 85% and 94% respectively. *E. coli* having a relatively higher MIC value shows 70% and 82% mortality during the same incubation period (Fig. 5). The mortality for *E. coli* and *S. aureus* was 99% for both CuNp and AgNp. Agar plates of the control and nanocomposite treated bacteria after 4 h are presented in Fig. 6.

3.5.3. Flow cytometry analysis

The internalization of PI, a non cell-permeant dye is used to distinguish between nanocomposite treated and untreated cells. This dye binds to DNA in dead or membrane compromised cells. The uptake of the dye both for untreated *S. aureus* and *E. coli* is very low, and remarkably increases for the CM and SM treated cells. In the case of *E. coli* the killing of CM and SM treated cells are 81.9% and 65.83% respectively whereas for *S. aureus* the values are 90.59% and 82.68% (Fig. 7). This result also substantiates the data obtained from bactericidal kinetics data.

3.5.4. MTT assay

The cell viability assay shows a substantial decrease in absorbance signifying a lower amount of formazan formation in case of CM, SM and nanoparticles treated cells of *E. coli and S. aureus* with respect to the untreated cells (Fig. 8a).

3.5.5. β-Galactosidase assay

Fig. 7b shows the absorbance due to β-galactosidase release. The result shows an increase in absorbance of about 13 and 27 folds for CM and SM respectively as compared to the untreated cells. The increase in activity of β-galactosidase corresponds to the rupture of inner membrane and release of cellular components by the effect of nanocomposite treatment (Fig. 8b).

3.5.6. ROS generation

The reactive oxygen species level in the cells treated with mullite, CuNp, AgNp, and the nanocomposites (CM and SM) were compared to the control i.e. the untreated cells. The level of ROS for the control cells was considered as 100%. There was a slight increase in ROS level in mullite treated cells,

For SM treated cells the intensity is about 5 times higher with respect to the control for both *E. coli* and *S. aureus*. For CM this increase is approximately 3 and 8 times for *E. coli* and *S. aureus* respectively (Fig. 9 a, b). The ROS level of CuNp treated cells were 7 and 10 folds higher than control for *E. coli* and *S. aureus* respectively, whereas the corresponding values for AgNp treated cells were 10 and 9 times respectively. As observed the oxidative stress in the CuNp and AgNp treated cells was much elevated as compared to the control and nanocomposite treated cells.

The fluorescence microscopic images show that untreated cells of *E. coli* and *S. aureus* are intensely stained with SYBR Green, whereas

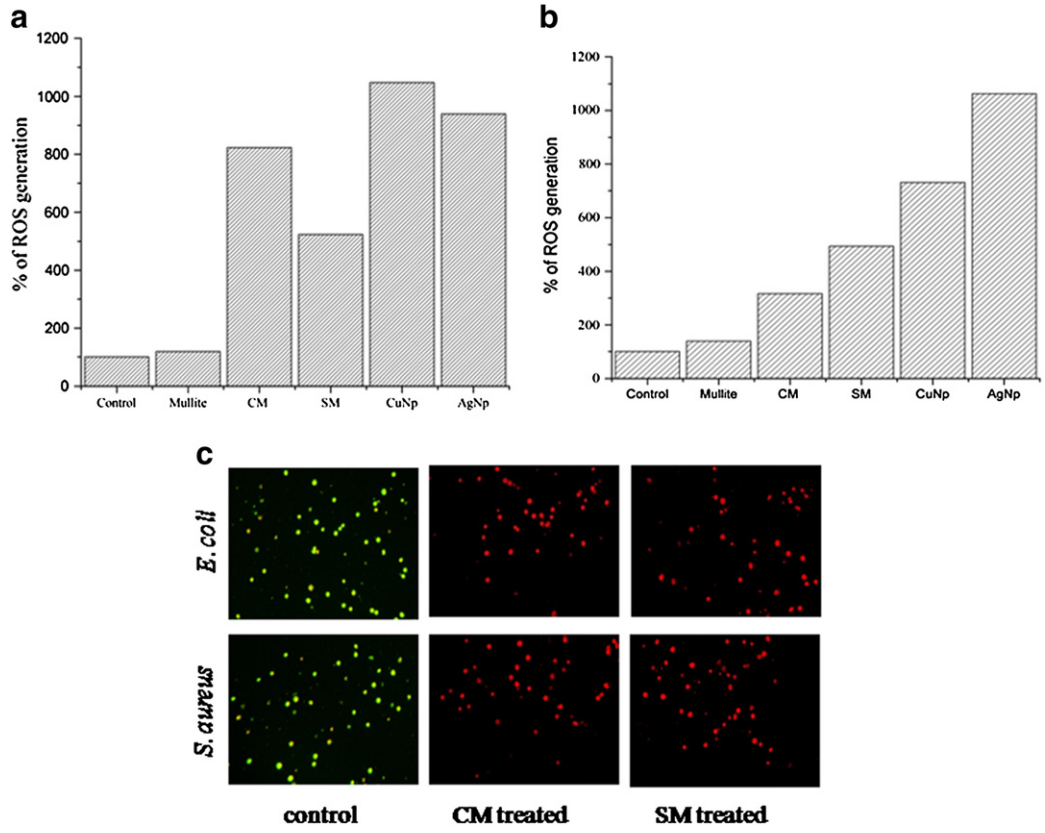

Fig. 9. Intracellular ROS generation measurement by DCFHDA for (a) *S. aureus* (b) *E. coli*. (c) Fluorescence microscopic images of control, CM and SM treated *E. coli* and *S. aureus* respectively by staining with SYBR Green/PI under 400× magnification.

the nanocomposite treated cells are found to be PI positive, demonstrating that these cells have lost their plasma membrane integrity (Fig. 9c).

3.5.7. EPR spectra

The EPR spectrum for CM (Fig. 10a) shows g near 2.054, which is very close to the value reported [17], indicating the presence of Cu^{2+} in the CM dispersed aqueous system. Since free radicals are of very short lifetime and spin trapping is needed to detect them by this method, no free radical signal is obtained. For SM the g value is around 2.052 [18] indicating the presence of Ag nanoparticle in the SM dispersed aqueous system (Fig. 10b).

3.5.8. Effect of nanocomposites on mammalian cell line

In the present investigation mouse fibroblast cells (L929) are chosen, as they are the typical cell type involved at the early stage of wound curing process in orthopedic fracture repair and is widely accepted based on evaluation of biocompatibility of materials [19]. The result indicates that the effects of nanocomposites are dependent on exposure time and concentration. When applied in identical concentration, the

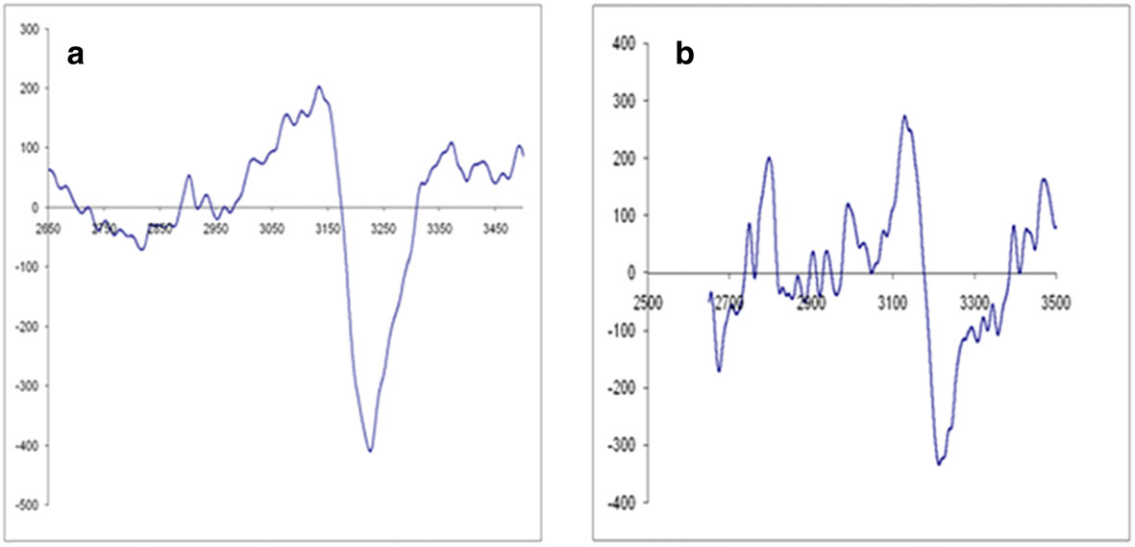

Fig. 10. EPR spectroscopy of (a) copper mullite (b) silver mullite dispersed in water.

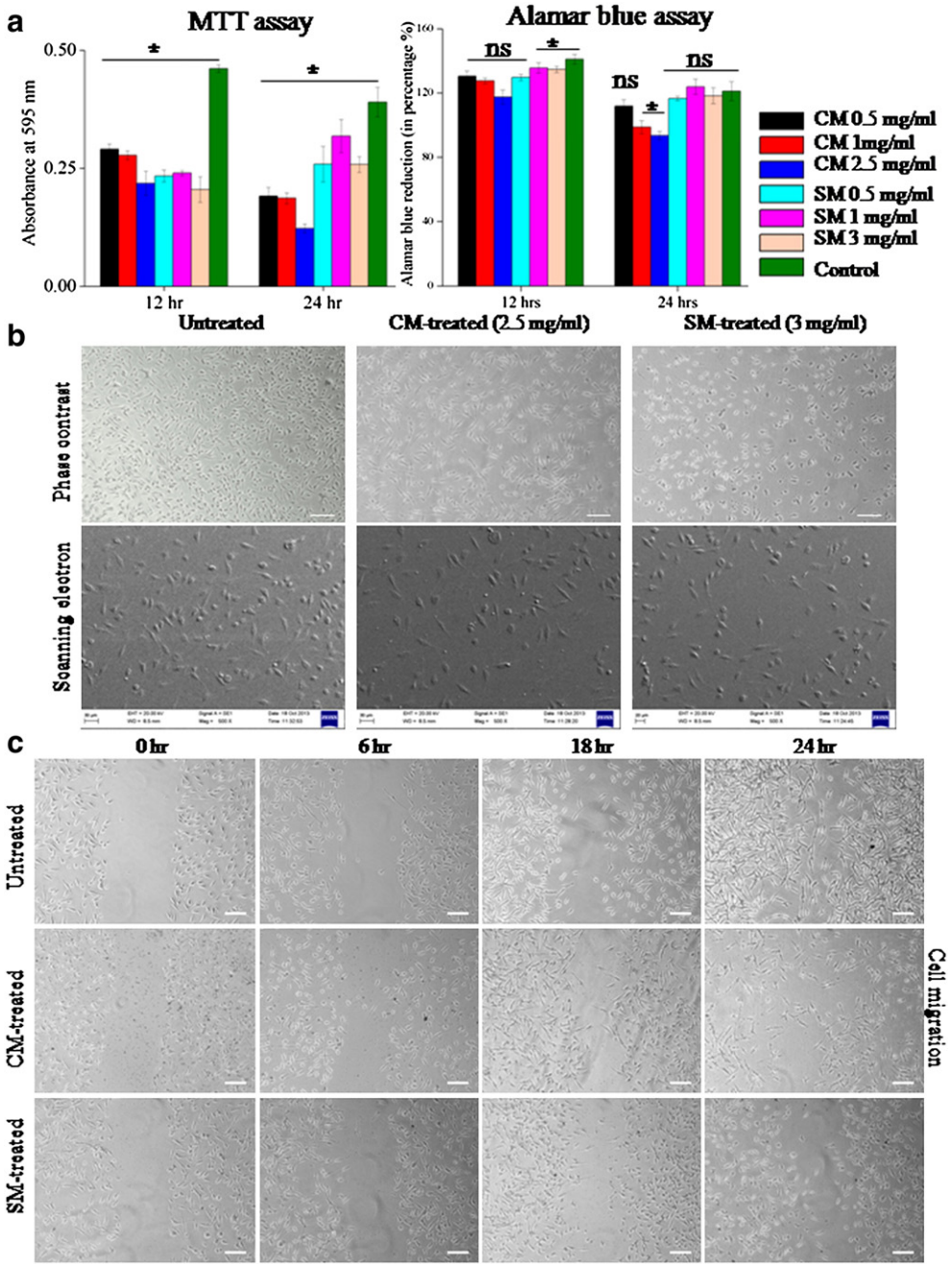

Fig. 11. Effect of nano-composites on (a) the cellular viability (MTT assay) and proliferation (Alamar blue assay) of mouse fibroblast cells (L929). The cellular viability and proliferation reduce with time in a dose dependent. Data are presented as mean ± SD (n = 3). ns = not significant and *p < 0.05 is considered as statistically significant from the control at the respective incubation time. (b) Phase contrast and scanning electron micrographs of appearance of L929 cells on glass cover slip after treatment with nano-composites. All cells (treated or untreated) reveal flattened morphology with multiple filopodia expanding in all directions. Cells are in great contact with each other. Scale bar represents 100 μm (phase contrast micrography).(c) Cellular migration-Scratch assay using L929 cells. The scratch is created using a sterile tip. Cells migrate well in presence of highest concentration of test composites (2.5 mg/ml for CM and 3 mg/ml for SM nanocomposites prepared in complete media) for a time period of 24 h. The patch is almost covered within 24 h by the treated cells and comparable to control (untreated cells). Scale bars represent 100 μm.

metabolic activity of CM treated cells after initial 12 h is more than that of SM treated cells and very close compared to control (Fig. 11a) (*p < 0.05). However, after 24 h increased metabolic activity is observed in SM treated samples; while both control and CM treated samples exhibit a reduction in cellular viability (Fig. 11a). The doubling time for L929 cells is 14 h [20]; therefore, cells exhibit high metabolic activity and reach confluence in CM and control plates. Due to limitation in surface area in 96 well plates, the cells start dying and demonstrate less viability or metabolic activity after 24 h [21]. The treatment with SM particles slows the initial proliferation rate of L929 cells, which allows these cells to reach confluence after 24 h. The rate of proliferation of cells is reduced slightly after 24 h and supports the MTT observation (*p < 0.05, ns = not statistically significant) (Fig. 11a). Cells retain their normal well stretched healthy morphology when observed under phase contrast and scanning electron microscopes (Fig. 11b). This is an indicator of cyto-compatibility of the test compounds. Furthermore, the cell scratch assay investigates the effect of the nanocomposites on the closure of a wound created artificially in L929 cell monolayer (Fig. 11c). After a repair period of 24 h at 37 °C, all the L929 cells (both treated and untreated) efficiently proliferate and migrate into the damaged area. Well developed filapodia are visible in most of the cells with a few mini-filopodia spread out, which is

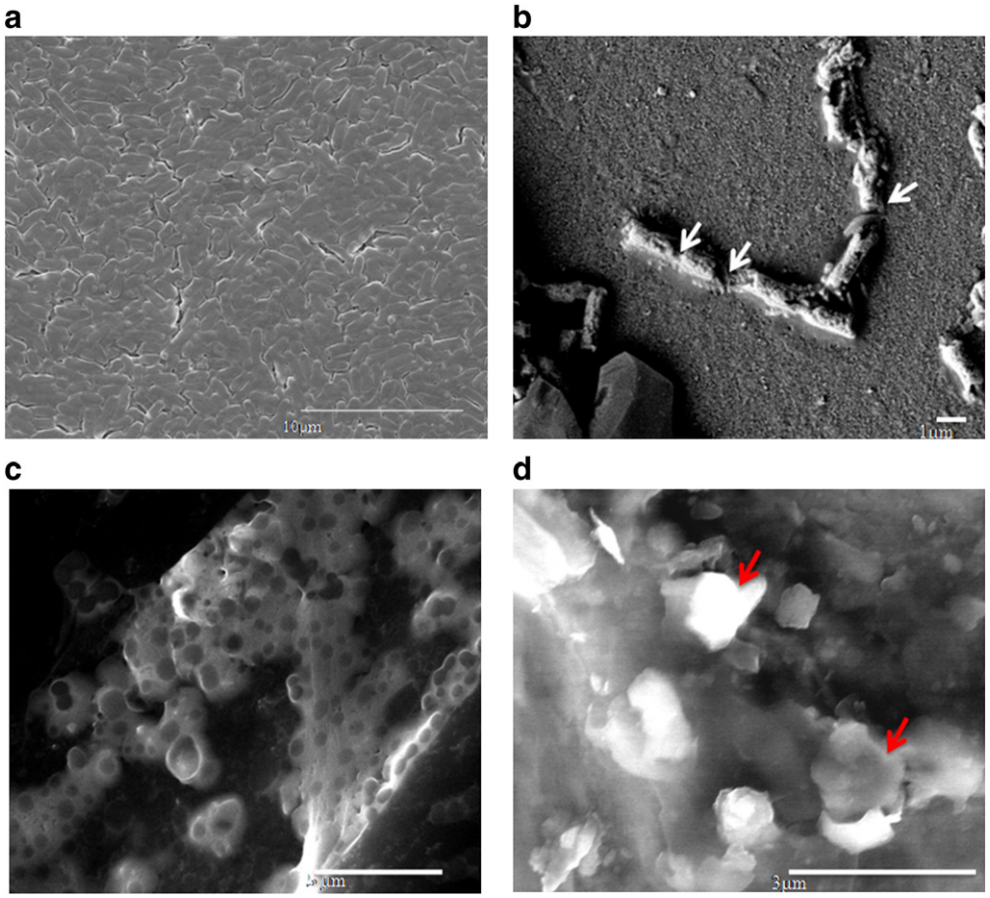

Fig. 12. FESEM images of control (a) *E. coli* and (c) *S. aureus* and nanocomposite treated (b) *E. coli* and (d) *S. aureus*. Membrane disruption is shown with arrows.

attributed to the spindle shaped structure of the cells. The observation indicates the absence of any adverse effect of the nanocomposites on cellular migration. The cell migration and the mobility of treated cells are comparable to those of control.

3.5.8.1. Mechanism of antimicrobial action. The antimicrobial property of silver/copper nanoparticles and their related compounds are being explored in detail by several groups. They are found to depend on several external factors like pH, temperature, aeration rate, concentration of nanoparticles and bacterial population [22,23]. Effect of silver nanoparticles against yeast, *E. coli* and *S. aureus* suggested their potential role as effective growth inhibitors, and thus may be applied to fabrication of diverse medical devices [22]. Strain specific antimicrobial activity of silver and copper nanoparticles was studied by Ruparelia et al. 2008 [24].

The generation of intracellular ROS is considered one of the factors for action of antibacterial agents containing silver nanoparticles [11], copper and copper derived nanoparticles [24]. Bacteria growing aerobically generate ROS as a metabolic by-product. The increase in the level of ROS within the cell exceeding an organism's detoxification and repair capabilities results in damage of DNA, RNA, proteins and lipids [25]. Kohanski et al. [26] reported that the ROS is involved in the process of microbial killing by three major classes of bactericidal antibiotics, regardless of drug–target interaction. The toxicity of copper is largely due to its tendency to alternate between its cuprous, Cu(I), and cupric, Cu(II), oxidation states, differentiating copper from other trace metals, such as zinc or nickel. Under aerobic conditions, this redox cycling leads to the generation of highly reactive hydroxyl radicals that readily and efficiently damage biomolecules, such as DNA, proteins, and lipids. Silver ions inactivate enzymes by binding sulfhydryl (thiol) groups in amino acids and promoting the release of ions with subsequent hydroxyl radical formation by an indirect mechanism likely mediated by reactive oxygen species.

Bacterial membranes possess a large percentage of anionic lipids such as cardiolipin and phospholipids containing phosphatidylglycerol [27,28]. Furthermore, bacteria have a more electronegative

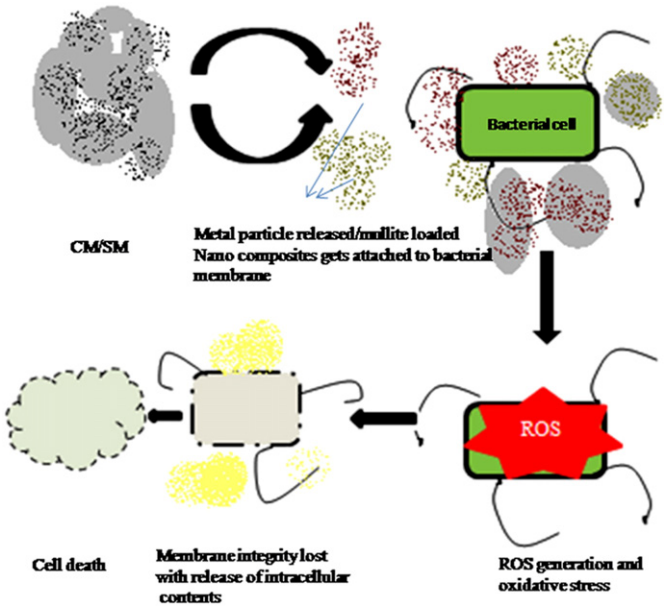

Fig. 13. Schematic representation of the phenomenon involved in killing of microbes by CM and SM nanocomposites.

transmembrane potential than eukaryotic cells and possess negatively charged constituents on their surface (e.g., lipopolysaccharide and lipoteichoic acids in Gram-negative and Gram-positive bacteria, respectively).

Several methods together share the phenomenon of antimicrobial killing by the mullite loaded silver and copper nanoparticles.

Firstly, the positively charged CTAB coated copper and silver nanoparticles that are released in the liquid growth medium are attracted electrostatically to the negatively charged cell wall of bacteria.

Secondly, a few oxidized silver and copper ions also get attached electrostatically to the bacterial membrane and get docked to their surface decreasing the osmotic stability of the cell, followed by subsequent leakage of intracellular constituents. The evidence of membrane disruption and the release of intracellular content can be understood from the SEM micrographs (Fig. 12) of the bacteria and β-galactoside assay respectively.

Finally the detrimental intracellular ROS generation also mediates the killing of bacteria. The biological targets for these highly reactive oxygen species are DNA, RNA, proteins and lipids. Free radicals attack membrane polyunsaturated fatty acids and initiate lipid peroxidation. Thus primary effect of lipid peroxidation is to decrease the membrane fluidity, which alters membrane properties and can disrupt membrane-bound proteins significantly [29]. The group of phenomena involved is schematically presented (Fig. 13).

The findings also indicate that the mullite–metal nanoparticle composite is relatively nontoxic below 1 mg/ml concentration and actually promotes proliferation of mouse fibroblast cells (L929) as observed by cell scratch assay.

4. Conclusions

In summary, a mullite–metal nanoparticle based antimicrobial nanocomposite system is developed for antibacterial therapeutic applications. Characterization of the nanocomposite indicates uniform distribution of spherical shaped nanoparticles, which are coated and are inside the inter granular spaces of mullite crystals. Strong anti-bactericidal activity is observed against *E. coli* and *S. aureus* by both copper (CM) and silver (SM) nanocomposites; with copper being more active, most probably due to the smaller particle size. The mechanism of antimicrobial action is primarily by three distinct steps: attachment of the nanocomposites on bacteria, interaction with free as well as surface coated metal nanoparticles and generation of ROS with consequent membrane disruption followed by cell death. Both the nanocomposites exhibit good cytocompatibility at a concentration of 1 mg/ml (MBC) with wound healing characteristics in mouse fibroblast cell line (L929).

Acknowledgment

We are grateful to the Department of Science and Technology, Govt. of India for financial assistance.

References

[1] M.J. Hajipour, K.M. Fromm, A.A. Ashkarran, D.J. de Aberasturi, I.R. de Larramendi, T. Rojo, V. Serpooshan, W.J. Parak, M. Mahmoudi, Antibacterial properties of nanoparticles, Trends Biotechnol. 30 (2012) 499–511.
[2] C. Marambio-Jones, E.M.V. Hoek, A review of the antibacterial effects of silver nanomaterials and potential implications for human health and the environment, J. Nanopart. Res. 12 (2010) 1531–1551.
[3] J. Ramyadevi, K. Jeyasubramanian, A. Marikani, G. Rajakumar, A.A. Rahuman, Synthesis and antimicrobial activity of copper nanoparticles, Mater. Lett. 71 (2012) 114–116.
[4] E. Bernardo, P. Colombo, E. Pippel, J. Woltersdorf, Novel mullite synthesis based on alumina nanoparticles and a preceramic polymer, J. Am. Ceram. Soc. 89 (2006) 1577–1583.
[5] S. Saleh, M.O. Taha, R.N. Haddadin, D. Marzooqa, H. Hodali, Preparation of silver- and zinc-doped mullite-based ceramics showing anti-bacterial biofilm properties, Molecules 16 (2011) 2862–2870.
[6] B. Bagchi, S. Dey, S. Bhandary, S. Das, A. Bhattacharya, R. Basu, P. Nandy, Antimicrobial efficacy and biocompatibility study of copper nanoparticle adsorbed mullite aggregates, Mater. Sci. Eng. C 32 (2012) 1897–1905.
[7] K. Yoshida, H. Hyuga, N. Kondo, H. Kita, Synthesis of precursor for fibrous mullite powder by alkoxide hydrolysis method, Mater. Sci. Eng. B 173 (2010) 66–71.
[8] J. Madejova, FTIR techniques in clay mineral studies, Vib. Spectrosc. (2003) 1–10.
[9] S. Joshi, G.S. Bisht, D.S. Rawat, A. Kumar, R. Kumar, S. Maiti, S. Pasha, Interaction studies of novel cell selective antimicrobial peptides with model membranes and *E. coli* ATCC 11775, Biochim. Biophys. Acta 1798 (2010) 1864–1875.
[10] I. Bajpai, K. Balani, B. Basu, Spark plasma sintered HA-Fe3O4-based multifunctional magnetic biocomposites, J. Am. Ceram. Soc. 96 (2013) 2100–2108.
[11] J. Miller, Experiments in Molecular Genetics, Cold Spring Harbor Laboratory, NY, 1972. 352–355.
[12] H.L. Su, C.C. Chou, D.J. Hung, S.H. Lin, I.C. Pao, J.H. Lin, F.L. Huang, R.X. Dong, J.J. Lin, The disruption of bacterial membrane integrity through ROS generation induced by nanohybrids of silver and clay, Biomaterials 30 (2009) 5979–5987.
[13] S. Barbesti, S. Citterio, M. Labra, M.D. Baroni, M.G. Neri, S. Sgorbati, Two and three-color fluorescence flow cytometric analysis of immunoidentified viable bacteria, Cytometry 40 (2000) 214–218.
[14] B. Kundu, S.C. Kundu, Silk sericin/polyacrylamide in situ forming hydrogels for dermal reconstruction, Biomaterials 33 (2012) 7456–7467.
[15] K. Wang, L. Cao, J. Huang, J. Fei, A mullite/SiC oxidation protective coating for carbon/carbon composites, J. Eur. Ceram. Soc. 33 (2013) 191–198.
[16] P. Padmaja, G.M. Anilkumar, P. Mukundan, G. Aruldhas, K.G.K. Warrier, Characterisation of stoichiometric sol–gel mullite by Fourier transform infrared spectroscopy, Inorg. Mater. 3 (2001) 693–698.
[17] W.B. Lewis, J.R.M. Alei, L.O. Morgan, Magnetic resonance studies on copper(II) complex ions in solution. I. Temperature dependences of the 170 NMR and copper(II) EPR linewidths of $Cu(H_20)62+$, J. Chem. Phys. 44 (1966) 2409–2417.
[18] R.A. Salkar, P. Jeevanandam, S.T. Aruna, Y. Koltypin, A. Gedanken, The sonochemical preparation of amorphous silver nanoparticles, J. Mater. Chem. 9 (1999) 1333–1335.
[19] S. Nath, B. Basu, M. Mohanty, P.V. Mohanan, In vivo response of novel calcium phosphate–mullite composites: results up to 12 weeks of implantation, J. Biomed. Mater. Res. B Appl. Biomater. 90B (1999) 547–557.
[20] K. Theerakittayakorn, T. Bunprasert, Differentiation capacity of mouse L929 fibroblastic cell line compare with human dermal fibroblast, World Acad. Sci. Eng. Technol. 50 (2011) 373–376.
[21] B. Kundu, P. Saha, K. Datta, S.C. Kundu, A silk fibroin based hepatocarcinoma model and the assessment of the drug response in hyaluronan-binding protein 1 overexpressed HepG2 cells, Biomaterials 34 (2013) 9462–9474.
[22] J.S. Kim, et al., Antimicrobial effects of silver nanoparticles, Nanomed. Nanotechnol. Biol. Med. 3 (2007) 95–101.
[23] F. Rispoli, A. Angelov, D. Badia, A. Kumar, S. Seal, V. Shah, Understanding the toxicity of aggregated zero valent copper nanoparticles against *Escherichia coli*, J. Hazard. Mater. 180 (2010) 212–216.
[24] J.P. Ruparelia, A.K. Chatterjee, S.P. Duttagupta, S. Mukherji, Strain specificity in antimicrobial activity of silver and copper nanoparticles, Acta Biomater. 4 (2008) 707–716.
[25] M.P. Brynildsen, J.A. Winkler, C.S. Spina, I.C. MacDonald, J.J. Collins, Potentiating antibacterial activity by predictably enhancing endogenous microbial ROS production, Nat. Biotechnol. 31 (2013) 160–167.
[26] M.A. Kohanski, D.J. Dwyer, B. Hayete, C.A. Lawrence, J.J. Collins, A common mechanism of cellular death induced by bactericidal antibiotics, Cell 130 (2007) 797–810.
[27] G.V. Meer, D.R. Voelker, G.W. Feigenson, Membrane lipids: where they are and how they behave, Nat. Rev. Mol. Cell Biol. 9 (2008) 112–124.
[28] M.R. Yeaman, N.Y. Yount, Mechanisms of antimicrobial peptide action and resistance, Pharmacol. Rev. 55 (2003) 27–55.
[29] E. Cabiscol, J. Tamarit, J. Ros, Oxidative stress in bacteria and protein damage by reactive oxygen species, Int. Microb. 3 (2000) 3–8.